Journal of the European Ceramic Society 43 (2023) 3600–3609

Contents lists available at ScienceDirect

Journal of the European Ceramic Society

journal homepage: www.elsevier.com/locate/jeurceramsoc

Crystallized fraction and crystal size effects on the strength and toughness of lithium disilicate glass-ceramics

M.V. Senk [a,*], I. Mathias [b], E.D. Zanotto [c], F.C. Serbena [a]

[a] Department of Physics, State University of Ponta Grossa (UEPG), Ponta Grossa, PR, Brazil
[b] Department of Mathematics, State University of Ponta Grossa (UEPG), Ponta Grossa, PR, Brazil
[c] Vitreous Materials Laboratory (LaMaV), Department of Materials Engineering, Federal University of São Carlos (UFSCar), SP, Brazil

ARTICLE INFO

Keywords:
Glass-ceramic
Fracture strength
Toughness
Lithium Disilicate

ABSTRACT

This work investigated the variation in fracture strength and toughness of stoichiometric lithium disilicate (LS2) glass-ceramics as a function of crystal size (d) and crystallized volume fraction (f), with three average crystal sizes (8, 13 and 34 μm) and a wide range of crystallized fractions (0–100 %). The fracture strength and toughness increased with increasing the crystallized volume fraction. For constant crystallized fraction, K_{IC} increased with crystal size, indicating an R-curve behavior. The mean free path between the crystals limits the maximum size of the critical defect and is the crucial feature controlling fracture strength. Finally, we verified that the contribution to the toughness of R-curve mechanisms in this glass-ceramic is proportional to $(f.d)^{1/2}$, which agrees with R-curve models for ceramics.

1. Introduction

Synthetic inorganic glasses were discovered about 6000 years ago. They have been intensively studied in the past decades because of their widespread applicability in everyday life and various areas of science and technology. While most physicochemical properties of glasses are highly positive, their inherent brittleness is not.

On the other hand, glass-ceramics (GCs) result from the controlled crystallization of one or more crystalline phases embedded in a residual glassy matrix [1], and generally present mechanical properties superior to those of their parent glasses. The greatest advantage of GCs is that they enable the large-scale production of materials with complex geometries (using all the available glass forming techniques) and tight microstructural control, thus with optimized mechanical strength, temperature resistance, and widely different but controllable thermal, chemical, electrical and optical properties [1]. A crucial aspect of GCs is that they present unique combinations of properties [2].

Stoichiometric lithium disilicate (LS2) is the main model glass-ceramic, as the precursor glass nucleates and crystallizes homogeneously throughout its volume, even with no nucleating agent. Thus, LS2 has been intensively studied [3,4]. Its crystal size (d) and crystallized volume fraction (f) depend on the heat treatment temperature and time [2–4]. The best nucleation temperature is well-known for this particular system, with the highest nucleation rate occurring at ~450 °C, and measurable crystal growth rates in the range of 430 °C to the melting temperature [4,5].

Some mechanical properties and residual stresses in stoichiometric LS2 GCs have already been measured [6,7]. However, these measurements were limited to relatively small crystallized volume fractions, or only the elastic modulus and bending strength were reported. Serbena et al. [8] comprehensively studied the effect of the crystallized volume fraction on toughness for a constant crystal size (13 μm). That study suggested that two possible factors impair the flexural strength of glass-ceramics: crack propagation in the glass matrix, generated by existing residual stresses, and spontaneous crack nucleation around the precipitates under loading. More recently, Sabino et. al. [9] analyzed the flexural strength of barium disilicate glass-ceramics varying the crystallized volume fraction and crystal size independently. For GCs containing small (5 and 10 μm) uncracked spherulites, the fracture strength increased with spherulite volume fraction and depended weakly on the mean free path, λ, between crystals. However, for GCs with large splintered spherulites (30 and 100 μm), the fracture strength depended strongly on λ. Both studies found that K_{IC} increases with increased crystallized volume fraction and larger crystal sizes. This is due mainly to the crystallization of a tougher phase, with no significant influence of the residual thermal stresses. The crystals lead to the formation of

* Corresponding author.
E-mail address: mvsenk@yahoo.com.br (M.V. Senk).

https://doi.org/10.1016/j.jeurceramsoc.2023.02.004
Received 29 November 2022; Received in revised form 2 February 2023; Accepted 3 February 2023
Available online 4 February 2023

bridges that trap the propagating cracks between the crystals. The greater the degree of crystallization, and the harder and stronger the crystals, the more difficult it is for the crack to penetrate those crystals.

In this work, we thoroughly investigate the fracture strength and toughness of this same glass-ceramic covering crystallized fractions from 0 % to 100 % by varying the crystal size and the crystallized volume fraction (f) independently. The experimental results are discussed as to what mechanisms control these properties.

2. Experimental procedure

A stoichiometric lithium disilicate ($Li_2O.2SiO_2$) glass was prepared by mixing 33.3 mol. % of the precursor powders (Li_2CO_3 - Synth 99.0 %) and 66.6 mol. % SiO_2 (Vitrovita - Zeta 2–99.5 %) in a rotating polyethylene bottle for 20 min. The batch was melted in an electric furnace at 1450 °C in a Pt crucible, cast and remelted three times for 2 h in air, and finally poured and pressed between solid stainless-steel plates. After the melt was cast for the third time, samples with thicknesses between 2.7 and 3 mm were obtained and annealed at 435 °C (20 °C below T_g) for 180 min and slowly cooled to relieve the residual thermal stresses generated during their fabrication. The specimens were cut using a diamond saw, polished with silicon carbide paper up to 1200 grit, and finished using a colloidal cerium oxide suspension. After polishing, all samples were submitted to thermal treatment at 435 °C for 2 h, followed by slow cooling to relieve the stresses induced by the cutting and polishing procedures.

Crystallization was performed using two-stage heat treatments - the first for nucleation and the second for crystal growth. These treatments were performed in a tubular electric oven with temperature control within ±1 °C. The nucleation and growth temperatures were 460 and 538 °C, respectively. The nucleation time was varied to obtain different crystallized volume fractions, and the growth time was varied to obtain crystals with three different average sizes: 8, 13 and 34 μm. The crystals have an ellipsoid shape and computed size calculated by the length of the longest axis. Crystallized volume fraction and crystal size were evaluated by analyzing several optical micrographs. At least 400 crystals were observed and measured to ensure reasonable statistical representation. The crystals revealed themselves after exposure to air for a few hours due to the differential effects of moisture on the crystals and the residual glass matrix.

The glass transition temperature, T_g, was measured in pieces of glass of ~50 mm in diameter using a differential scanning calorimeter (DSC; model LABSYS EVO DTA/DSC), with a heating rate of 10 °C/min in the temperature range of 23–1100 ºC. The crystalline phases were identified using X-ray diffraction (XRD) and a Rigaku Ultima IV X-ray diffractometer in Bragg-Brentano geometry and θ-θ configuration. The XRD diffractograms were obtained using glass powder samples with different crystallized volume fractions, with Cu-K_α radiation in the 5°−80° 2θ range with 0.02° steps and a scan rate of 2°/min at 21 °C.

The flexural strength was measured using the ball on three balls (B3B) technique [10]. The jig consisted of three balls and a fourth ball centralized over the sample. The jig was made of stainless steel and alumina spheres with 4 mm radius. The samples were 1.2 ± 0.3 mm thick discs, with diameter of 12 ± 0.4 mm. All samples were cut from the glass, ground, and polished. After that, they were heat treated for the desired crystallized volume fraction and crystal size followed by slow cooling. Just before being tested, the samples were re-polished in aqueous CeO_2 suspension on both sides to remove the crystallized surface layer. The load was applied with a displacement rate of 500 μm/min using a universal mechanical testing machine (AGS-X 5 kN, Shimadzu). Three samples were tested for each crystallized volume fraction and crystal size.

The fracture strength (σ_S) was calculated as [1]:

$$\sigma_S = f(\alpha', \beta, \nu)\frac{F}{t^2} \tag{1}$$

where F is the applied load at fracture, t is the sample thickness, and f is a dimensionless factor that depends on the ratio of the sample thickness to the sample radius R, ($\alpha' = t/R$), R_S to the sample radius, ($\beta = R_S/R$), and the Poisson's ratio, ν [10].

The fracture toughness (K_{IC}) was measured using pre-cracked beam specimens in 4-point bending. The separations between the inner and outer rollers were 10 and 20 mm, respectively. Samples with the desired crystallized volume fraction and crystal size were prepared in the same way as those for the fracture strength tests. The sample dimensions were 2 × 2×25 mm^3. The pre-crack was prepared by indenting the surface with a 10 N Vickers diamond indenter over its full width, as shown in Fig. 1a) The distance between the indentations was 100 μm to produce a long and sharp pre-crack running across the whole sample. Fig1b) shows an optical micrograph of the fractured surface after the four-point bending test. This sample has a crystalline fraction of 24 % and an average crystal diameter of 34 μm.

To relieve the indentation-induced residual stresses, all samples were annealed at 435 °C for 2 h, followed by slow cooling. Subsequently, the four sides of the samples were polished with an aqueous CeO_2 suspension to remove the crystallized crust and then tested. The typical relaxation time, τ, at T_g is ~100 s for any oxide glass. From the Maxwell relation, $\tau = \eta/G$, where η and G are the glass viscosity and shear modulus, respectively, we can estimate the time for stress relief due to viscous flow. Using data from Zanotto and James [11], the estimated viscosity for the LS2 glass at 435 °C is 5.1 × 10^{13} Pa.s. The glass shear modulus can be estimated from $G = E/2(1+\nu)$. Using the well know experimental value of E = 75 GPa and $\nu = 0.22$, G = 30.7 GPa. Therefore, the estimated relaxation time τ at 435 °C is ~30 min; which is much shorter than the 2 h experimentally used.

The load was applied at a displacement rate of 500 μm/min using a universal mechanical testing machine (AGS-X 5 kN, Shimadzu). A minimum of three samples were tested for each condition. The tests were performed at room temperature and relative air humidity of 65 %.

The fracture toughness was calculated as [12]:

$$K_{IC} = \frac{3YF(L-l)\sqrt{\alpha}}{2bh^{3/2}(1-\alpha)^{3/2}}, \tag{2}$$

where

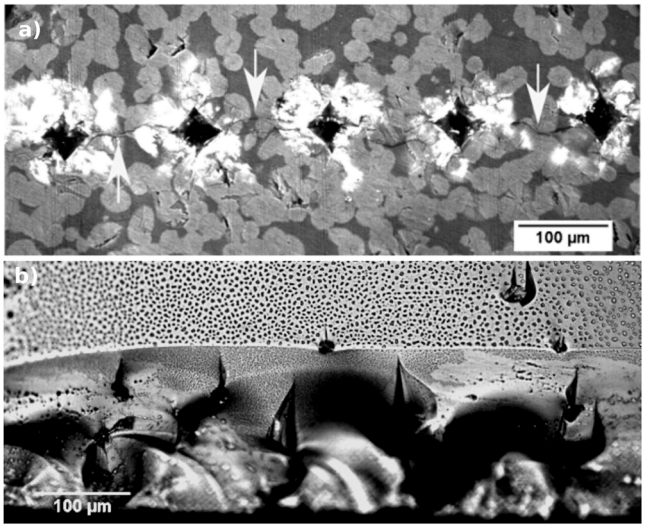

Fig. 1. Optical micrograph a) of a series of 10 N Vickers indentations used to introduce a pre-crack in the top surface of a 62 % crystallized GC with 13 μm crystals. The arrows indicate the radial cracks propagating from the indentations and b) crack front in a fractured surface of a sample with a crystalline fraction of 24 % and an average crystal size of 34 μm, after a four-point bending test.

$Y = 1.9887 - 1.326.\alpha - (3.49 - 0.68.\alpha + 1.35.\alpha^2).\alpha(1-\alpha)/(1+\alpha)^2$ and $\alpha = a/h$, where a is the depth of the pre-crack, h is the sample thickness, b is the sample width, F is the load at fracture, and L and l are the upper and lower support separations, respectively. The crack lengths were measured on the fractured surfaces by optical microscope, OM, (Olympus BX53M) after the tests. We also revisited some samples with different f fractured in a previous study [8] and observed the crack path and its interaction with crystals using OM. Thus, the different toughening mechanisms that operate at different crystallized volume fractions could be identified.

3. Results

3.1. Nucleation and crystal growth

Fig. 2(a-c) show the crystals nucleated in samples with 34 %, 32 % and 24 % crystallized volume fractions after removal of the crystallized surface layer, respectively for the three crystal sizes of this work. The crystals are slightly elongated, with long-to-short axis ratios of 2.3, 1.6 and 1.3 for the 8, 13 and 34 μm crystal sizes, respectively.

Fig. 3 shows a DSC trace of a small glass piece. The T_g onset is 455 °C, which is very close to the T_g of other stoichiometric LS2 glasses previously reported, e.g., [5,13]. One exothermic and one endothermic crystallization peak, corresponding to the melting of the crystallized glass, are also observed.

Diffractograms comparing small pieces of three LS2 GC samples are shown in Fig. 4: a) shows the typical amorphous background, referring to the parent glass sample with no heat treatment; b) and c) show crystallization peaks of $Li_2Si_2O_5$, which has an orthorhombic unit cell of the Ccc2 space group. These data also agree with the literature [3,14].

3.2. Fracture strength

Fracture strength measurements using the B3B method were performed with samples having different crystallized volume fractions and crystal sizes. The results are shown in Fig. 5.

For all crystal sizes tested, with a small crystallized fraction, ~4 %, the fracture strength for the glass increases 40 %, from 120 to 170 MPa. Then it increases continuously but less intensively, with further crystallization, reaching almost 300 MPa for the two smallest crystal sizes, and ~200 MPa for the GC with 34 μm crystals. In general, for a constant f, the strength for the two smallest crystals is larger than that for the largest crystals. The strength curves are quite similar for the 8 and 13 μm crystal sizes; however, for the 34 μm crystal size, there is a decrease of 27 % in relation to the other sizes.

In a previous work, Serbena et al. [8] measured the fracture strength of LS2 GCs in a 4-point bending experiment for a constant average crystal size of 12 μm, with f varying from 0 % to 100 %. The strength varied from 103 ± 3 MPa for the parent glass to 260 ± 20 MPa for the fully crystallized sample. They observed the same trends shown in Fig. 5: an abrupt increase in strength as soon as a small crystallized volume

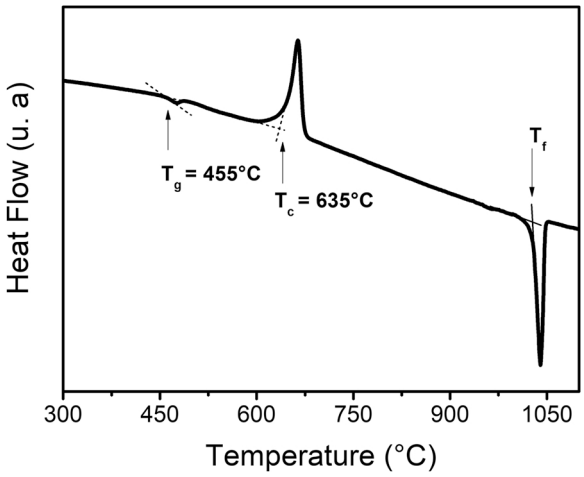

Fig. 3. DSC trace of a small piece of the LS2 glass. The glass transition temperature is 455 °C, the crystallization onset occurs at 635 °C and the melting onset at 1027 °C.

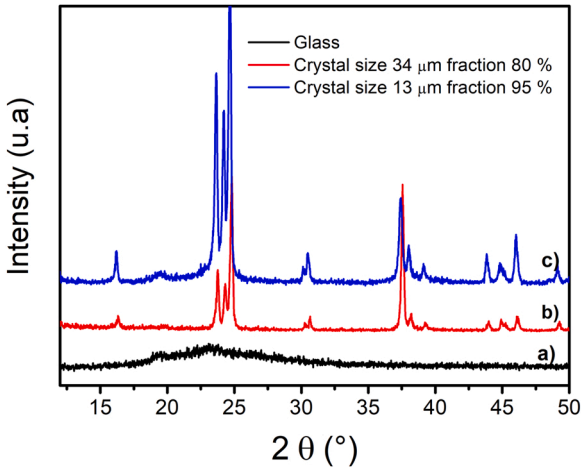

Fig. 4. XRD of a) parent glass, b) sample heat treated for 10 h at 460 °C + 4.5 h at 538 °C corresponding to a crystal size of 34 μm and crystallized volume fraction of 80 %, and c) sample heat treated for 127 h at 460 °C + 2 h at 538 °C with a crystal size of 13 μm and crystallized volume fraction of 95 %.

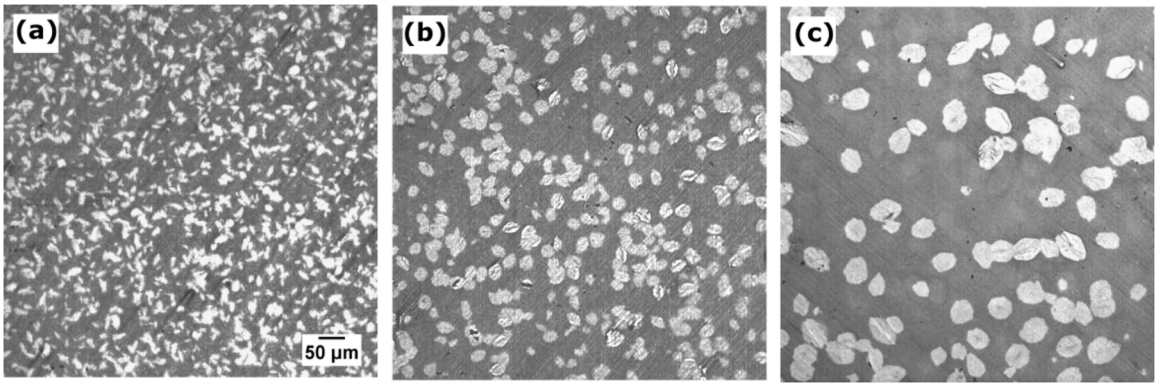

Fig. 2. Partially crystallized LS2 samples heat treated for (a) 207.5, (b) 35 and (c) 3.5 h at 460 °C for crystal nucleation, and for (a) 0.9, (b) 2 and (c) 4.5 h at 538 °C for crystal growth, corresponding to crystal sizes and crystallized volume fractions of 8 μm - 34 %, 13 μm - 32 % and 34 μm - 24 %, respectively.

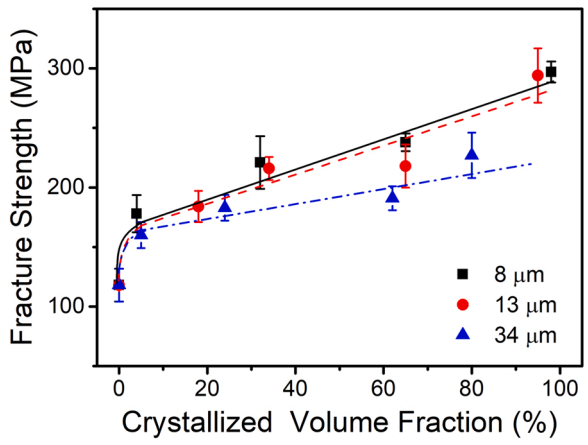

Fig. 5. Fracture strength as a function of the crystallized volumetric fraction for the LS2 GC with different crystal sizes. The lines are only a guide to the eyes.

fraction formed, with a continuous but less intense increase with further crystallization. Fig. 6 shows the comparison of their measurements with those of this work for a very similar average crystal size, which shows the effect of the experimental technique used to compute the strength values. This difference is related to the different effective volumes under tensile stress with distinct techniques and sample/crack geometries.

3.3. Fracture toughness

Fig. 7 shows K_{IC} as a function of the crystallized volume fraction for different crystal sizes. K_{IC} increases with increasing crystallized volumetric fraction and grain size, whereas an opposite dependence is observed for the fracture strength. K_{IC} was 0.8 ± 0.1 MPa.m$^{1/2}$ for the glass and 3.1 ± 0.2 MPa.m$^{1/2}$ for the GC with 34 μm crystal size and crystallized fraction of 80 %, - a substantial increase of 280 %. There is a strong initial increase of K_{IC} for the sample with a crystallized fraction of 5 % and 34 μm crystal size, reaching 1.5 MPa.m$^{1/2}$, an increase of 70 % over the parent glass. This increase with low f was not observed for glass-ceramics with 8 and 34 μm crystals.

Serbena et al. [8,15] have also measured the K_{IC} for LS2 GCs by the double-torsion technique, with an average crystal size of 12 μm for crystallized volume fractions varying from 0 % to 100 %. Fig. 8 compares the K_{IC} measured in this work with that of Serbena et al. [8] using a different technique. Both measurements show an (approximate) linear

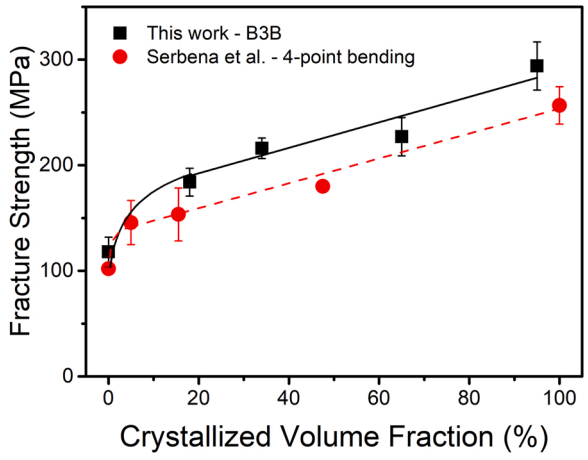

Fig. 6. Comparison of the fracture strength of LS2 GCs measured in this work by the B3B technique with those of Serbena et al. [8] using 4-point bending for similar average crystal sizes of 13 and 12 μm, this work and Serbena et al., respectively. The continuous curves are only guides to the eyes.

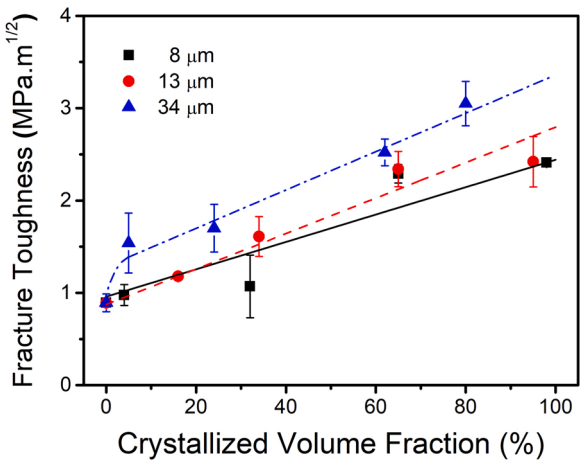

Fig. 7. Fracture toughness measured using pre-cracked beam test specimens with a sharp straight-through crack in the 4-point bending mode as a function of the crystallized volume fraction for different crystal sizes. The lines are only guides to the eyes.

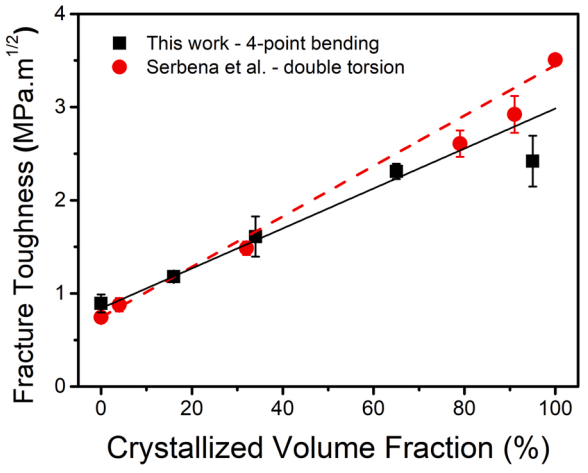

Fig. 8. Comparison of K_{IC} values measured in this work using pre-cracked beam test specimens of LS2 GCs with a sharp straight-through crack in the 4-point bending mode with those measured by Serbena et al. [8] using the double-torsion technique. The results are plotted as a function of the crystallized volume fraction for very similar crystal sizes (12–13 μm). The lines are the best linear fits to the experimental data.

increase of K_{IC} with increasing f, with differences < 28 %.

4. Discussion

4.1. Flexural strength

In most GCs, the crystals are usually anisotropic and present properties different from those of the vitreous matrix; hence, during cooling to ambient temperature, either tensile or compressive internal residual stresses are generated. Mathias [15] measured the thermal expansion coefficients (TECs) of the LS2 glass (12.2 ×10^{-6} °C^{-1}) and the crystals (average = 10.1 ×10^{-6} °C^{-1}) [6]. As the average TEC of the crystal is smaller than that of the vitreous matrix, the matrix generates compression on the crystals. Other factors that contribute to the residual stress intensity are the crystal shape anisotropy and the crystallized volume fraction.

We present below a review of some relevant studies on the mechanical properties of LS2 GCs. Li et al. [16] studied the effects of crystal size on the mechanical properties of LS2 GCs using the 3-point bending

technique. The crystals had lath-shaped crystals ranging from 0.6 to 3.3 μm in length. From fractography images, they observed that the larger crystals produced rougher fractured surfaces, and clearly exhibit a more effective blocking effect on crack propagation than the smaller crystals.

Huang et al. [17] produced a high-strength LS2 GC from a SiO_2–Li_2O-CaO-P_2O_5-ZrO_2 glass. They studied the influence of annealing and crystallization temperatures on the microstructure, indentation fracture toughness, and 3-point bending strength. They observed that increasing the crystallization temperature decreased the flexural strength from 440 to 300 MPa, whereas the indentation fracture toughness increased from 0.9 to 1.3 MPa.$m^{1/2}$. This increase was explained by the fact that the higher the crystallization temperature, the higher the LS2 crystal size.

Villas-Boas et al. [18] analyzed the effect of residual stress on the indentation fracture toughness of LS2 GCs. Their GCs contained crystals from 1 to 5 μm and crystallized volume fraction from 52 % to 78 %. The GCs were designed so that the TEC of the residual glassy matrix was lower, approximately equal, and higher than the average TEC of the LS2 crystal phase. In this way, the average residual stresses in the crystals would (theoretically) be tensile, null, and compressive. However, the experimental average residual stresses in the crystals measured by XRD were compressive or null (−100 to ~0) and highly anisotropic. For these relatively low residual stress levels, no significant effect on the fracture toughness was detected. The GC showing the highest fracture toughness had ~5 μm crystals, a high crystallized volume fraction (59 %), and a high modulus of elasticity (98 GPa); hence the microstructural effect prevailed over the residual stress.

The flexural loading technique has long been a basic test to determine the fracture resistance of ceramics and glasses. However, to the best of our knowledge, no systematic investigation has been conducted on the effects of the crystallized volume fraction on the strength of LS2 GCs with independent grain size variation. Most previous studies were performed with non-stoichiometric LS2 GCs with addition of several other elements, and with microstructures consisting mostly of elongated crystals of a few micrometers and crystallized fractions ranging from 30 % to 80 % [14,19,20]. Serbena et. al. [8] investigated the mechanical strength of LS2 using 4-point bending and fracture toughness measurements, varying the crystallized volumetric fraction for a constant crystal size of 12 μm. The fracture strength increased approximately 40 % for the sample with $f = 5$ % in relation to that of the parent glass, and 2.5 fold for a fully crystallized sample.

The simplest model for calculating the residual stresses within the crystals and the matrix/crystal interface, in glass-ceramics with spherical isotropic crystals and low crystalline fraction (<15 %), was proposed by Selsing [6,21]. Later on, Mori and Tanaka [22] and Hsueh and Becker [23] extended the Selsing's model and proposed an equation for the residual stress considering the crystallized fraction. The residual stress in a spherical precipitate (σ_p) is given by:

$$\sigma_P = \frac{\Delta\alpha.\Delta T}{\frac{1}{3K_C} + \frac{1}{4(1-f)G_g} + \frac{f}{3(1-f)K_g}}, \tag{3}$$

where G is the shear modulus, K is the compressibility modulus, f is the crystallized volume fraction, and E is the elastic modulus, and the indices g and c refer to the vitreous matrix and the crystal, respectively. The elastic moduli of the glass matrix (E_g) and the crystal (E_C) are 75 and 122 GPa, respectively. The Poisson's ratios for the glass and crystal are 0.22 and 0.19, respectively [6,15]. If $f = 0$, Eq. (3) becomes the Selsing's equation.

The average residual stress in the glass matrix has the opposite sign and is given by the equilibrium condition$f\sigma_C + (1-f)\sigma_g = 0$. Eq. (3) shows that as the crystallized volumetric fraction increases, the mean tensile residual stress in the residual glass increases linearly, regardless of the crystal size. The opposite occurs for the compressive stress in the crystal, which decreases with increasing f. In the glass matrix surrounding the crystals, the radial component of the stress is compressive whereas the tangential components are tensile. Both decay with distance from the crystal interface as $1/r^3$. It is important to note that the thermal residual stresses are affected by the thermal and elastic anisotropy and crystal shape.

There are two possible mechanisms controlling the flexural strength of our samples: (i) crack propagation in the glass matrix, which is aided by the residual tensile stress but is limited in size due to the limited distance between the crystals, and (ii) crack nucleation around the crystals induced by the residual and external stresses.

The first mechanism is associated with the average distance between the crystals, which limits the maximum defect size assumed to be in the residual glass, which is the phase with the lowest fracture toughness. If we assume that the critical defect is a semicircular crack of radius $\boldsymbol{c}$, the relation $\sigma_S = 0.78K_{IC}.c^{-1/2}$ should hold [24]. Then a good estimator of this distance is the mean free path, λ [25]:

$$\lambda = \frac{2d(1-f)}{3f} \tag{4}$$

where d is the crystal diameter and $c = \lambda/2$.

Fig. 9 shows the fracture strength variation with $\lambda^{-1/2}$. The relation is approximately linear and independent of crystal size up to $f = 80$ %. This result indicates that the distance between the crystals controls the maximum defect size, and is independent of crystal size. The crystals block the growth of the cracks and limit their size. The inset displays the full range of $\lambda^{-1/2}$ variation with samples with crystallized volume fractions of 95 % and 98 %, where the fracture strength reaches a constant value. This behavior is likely related to existing defects in the crystalline phase, and not to defects in the glass matrix.

Therefore, the fracture strength is related to the crystal mean free path as:

$$\sigma_S = \sigma_S^g + C'.\lambda^{-1/2}, \tag{5}$$

where σ_S^g is the fracture strength of the residual glass and C is a constant. From Eqs. (4) and (5) can be rewritten as:

$$\sigma_S = \sigma_S^g + C.\sqrt{\frac{f}{1-f}}.d^{-1/2}, \tag{6}$$

where C is a constant that depends on the GC fracture toughness, sample size and loading conditions. In this way, an explicit dependence of fracture strength on f and $d^{-1/2}$ is obtained.

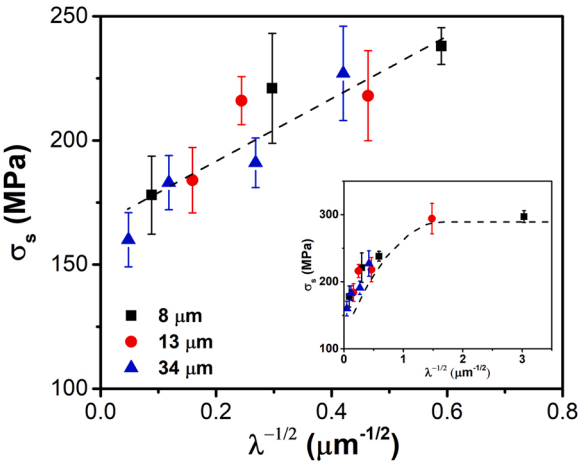

Fig. 9. Fracture strength variation with the mean free path. The highest data point is for $f = 80$ %. The inset shows the variation including the highest crystallized volume fractions of 95 % and 98 %. The lines are only a guide to the eyes.

Fig. 10 shows the simulations of the σ_S variation with $\boldsymbol{f}$ predicted by Eq. (6) with $C = 0.35$ MPa.m$^{1/2}$. The dependence on crystal size is revealed and the agreement is reasonable. The predicted curves for the 8 and 34 μm crystal sizes encompass all experimental data. At low f, the predicted values are lower than the experimental data, especially for the 34 μm size crystals. For $\boldsymbol{f}$ between 20 % and 65 %, the agreement is reasonable.

The second possible mechanism of crack nucleation around the crystals induced by external and thermal residual stresses was described by Green [25]. It refers to a spherical precipitate with an R radius under compressive residual stress σ_P, and an applied remote stress σ_S. The precipitate is surrounded by an annular crack with width $\boldsymbol{a}$ at its interface with the matrix perpendicular to σ_S. The critical radius R_C for spontaneous microcracking is:

$$R_C = \frac{\pi (K_{IC}^{gc})^2 (\alpha - 1)^5}{\alpha \left[2\sigma_S (\alpha + 1)^2 - \sigma_P\right]^2 (\alpha + 2)}, \tag{7}$$

where α a geometric factor equal a/R.

If we consider the maximum possible size of the annular crack as equal to the distance to the next precipitate, we can assume $\boldsymbol{a} = \lambda$. Therefore, combining Eqs. (4) and (7):

$$\sigma_S = \sqrt{\frac{3\pi}{2}\frac{f(f+2)}{(1-f^2)}}\frac{K_{IC}^{gc}}{\sqrt{d}} + \sigma_P \frac{9f^2}{(f+2)^2}, \tag{8}$$

where σ_P is given by Eq. (3). Again, a dependence of σ_S with $d^{-1/2}$ is predicted. A plot of σ_P variation with $\boldsymbol{f}$ for the different crystal sizes is shown in Fig. 11. The calculated σ_P are well above the experimental data, indicating that the microcracking mechanism proposed by Green does not operate in these LS2 GCs.

4.2. Fracture toughness

Observation of the fracture path revealed different toughening mechanisms acting in these GCs with different crystallized volume fractions, as shown in Fig. 12 (a-f). Crack deflection was always present, and its proportion increased with increasing f. Fig. 12(a) shows a crack arrested at a crystal, indicating that the crystals, indeed, act as pinning sources for crack propagation. At low f values, crack bowing and trapping by crystals were observed at the fracture plane, as displayed in Fig. 12(b). For larger f values, e.g., at 32 %, when the percolation threshold of the crystallized phase has been reached, crack bridging and branching are also observed, as shown in Fig. 12(c). Fig. 12(d) shows crack arrest by crystals and crack closure when the crack cuts a crystal. The closure can be the result of the higher elastic modulus of the crystals and the related compressive residual stresses (within the crystals). These

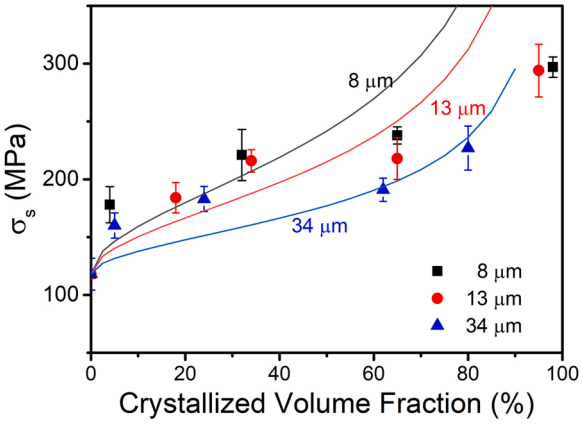

Fig. 10. Fracture strength variation with the crystallized volume fraction and the simulated curves according to Eq. (6) with $C = 0.35$ MPa.m$^{1/2}$.

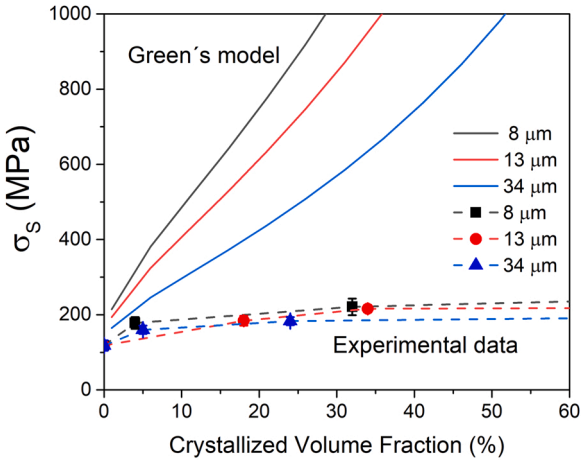

Fig. 11. Variation of fracture strength with crystallized volume fraction as predicted by Eq. (8).

residual stresses result from the different thermal expansions of the residual glass and the crystalline phase and arise during cooling after thermal treatment. They were estimated to be −60 MPa [7] in the crystals of low crystallized volume fraction LS2 GCs. At even higher crystallized volume fractions, cracks propagate preferentially along the elongated glass islands that are under tensile residual stresses, as shown in Fig. 12(e). At much higher $\boldsymbol{f}$ values, crack bridging and branching are observed once more (Fig. 12(f)).

We can identify roughly three different regimes as a function of increasing crystallized volume fraction for a constant crystal size. The boundaries are not rigidly fixed, but there is a smooth transition from one regime to another. These mechanisms are described in Fig. 13.

i. Glass matrix with isolated precipitates ($0 < f \lesssim 30$ %)

In this case, the crystallized volume fraction is smaller than the threshold for crystal percolation. The crystals are isolated and surrounded by the glass matrix. As $\boldsymbol{f}$ increases, two or three crystals may join to form a larger precipitate. The residual stresses are higher in the crystals and decrease as $\boldsymbol{f}$ increases. Possible toughening mechanisms include crack deflection, crack branching, crack bowing, crack trapping and bridging. A crack follows a path according to the highest tensile components of the residual stress field in the residual glass and may penetrate the crystal depending on the K_{IC}^c/K_{IC}^g ratio. If the crystals are cut by the crack during fracture, the crystal fracture toughness contributes to the overall K_{IC}^{gc} of the GC. Larger crystals may promote spontaneous microcracking and crack propagation can be arrested in the crystals. The glass contributes the most to the K_{IC}^{gc} of the GC.

ii. Two interpenetrating networks - glass and crystals ($30\ \% \lesssim f \lesssim 70\ \%$)

This situation occurs is when $\boldsymbol{f}$ is between the percolation thresholds for the crystalline and glass phases. Each phase forms a complete interconnected network. The residual stresses in each phase are approximately the same but with opposite signs, then crack deflection is observed. If the crystal is penetrable by a crack, crack bowing may occur. As the glass matrix fraction is reduced, there is more crack bridging and trapping. As each phase forms an interconnected network, the crack will break both the glass and the crystalline phases, increasing the contribution of the crystal toughness to the overall toughness of the GC. Thus, a weak R-curve behavior is observed. Both residual glass and crystals contribute in approximately equal amounts to the overall toughness of the GC.

iii. Crystallized matrix with isolated residual glass elongated islands ($70\ \% \lesssim f < 100\ \%$):

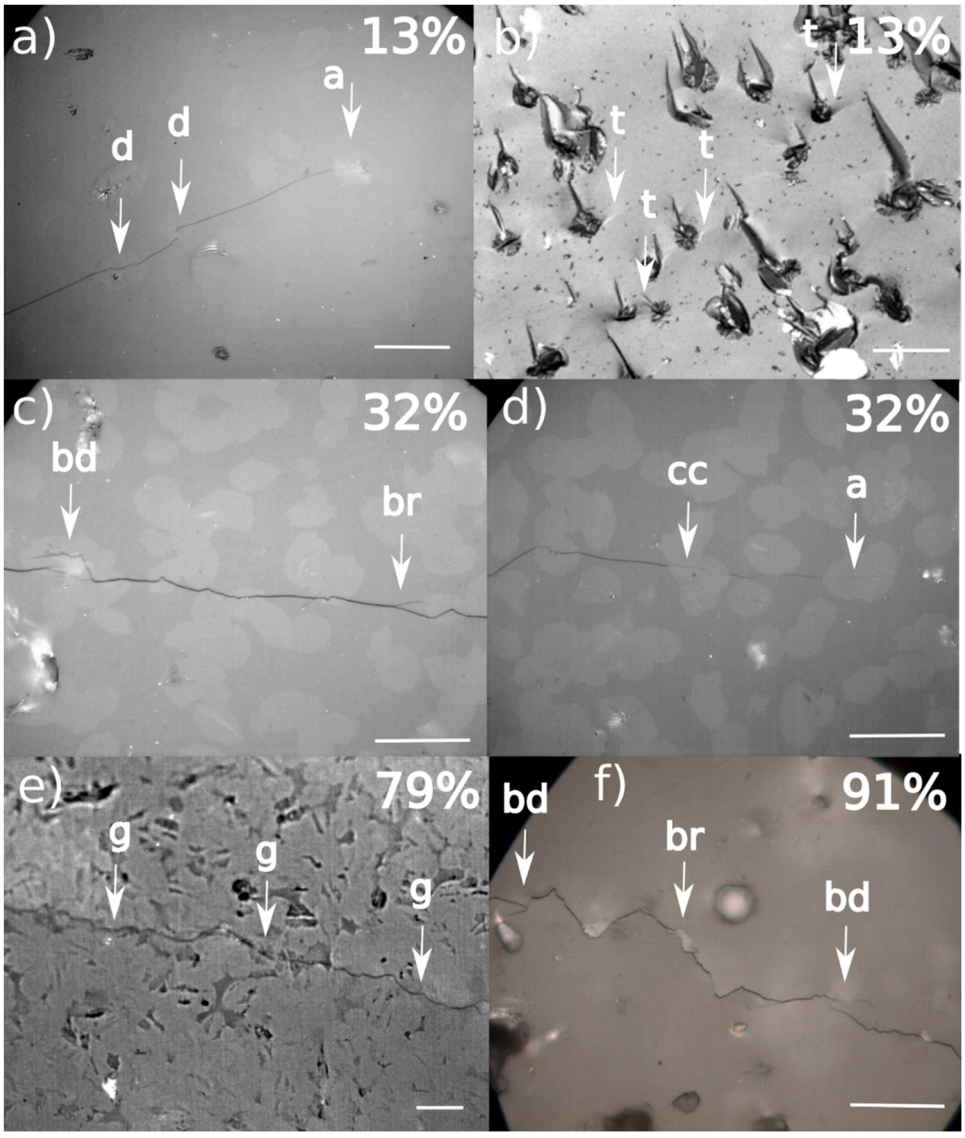

Fig. 12. Optical micrographs showing crack toughening mechanisms, indicated by arrows, in LS2 GCs with different crystallized volume fractions: a) crack deflection (d) and crack arrest (a) at a crystal ($f = 13$ %); b) crack trapping and bowing (t) in the fracture surface ($f = 13$ %); c) crack bridging (bd) and crack branching (br) ($f = 32$ %); d) crack closure (cc) in the crystal and crack arrest (a) at the precipitate ($f = 32$ %); e) crack path following mostly the elongated glass islands (g) that is under tensile residual stresses ($f = 79$ %); f) crack deflection, crack bridging (bd), and crack branching (br) ($f = 91$ %). Crystals are lighter and the glass matrix is darker. *Scale bars*: 20 μm.

This case occurs when the crystallized volume fraction, ***f***, is above the glass percolation threshold. The microstructure consists of a continuous crystalline network with a few glass islands. The glass is under higher residual stresses than the crystalline phase. In this case, the main toughening mechanisms are crack deflection and crystal bridging. The crack path tends to connect glass islands that are under tensile residual stresses in the case of LS2 GC. The precipitate fracture toughness predominantly contributes to the overall $K_{IC}^{gc}$of the GC. A stronger *R*-curve behavior is observed and the largest crystals enhance the *R*-curve. However, larger glass islands may promote cracking in LS2 GCs.

The main toughening mechanisms as a function of the crystallized volume fraction in LS2 GCs for a constant crystal size were discussed in detail in [8]. Here, we concentrate on the discussion about the effect of varying the crystal size on fracture toughness.

The model of Faber and Evans [26] considers the twisting and tilting of the crack front when it encounters a rigid precipitate. Different mode loadings are activated, leading to an increase in fracture toughness. The toughness increase depends on the crystallized volume fraction, precipitate shape, and on the interparticle distance between them, but not on precipitate size.

The model of Bower and Ortiz [27] considers crack bridging and trapping by precipitates left behind the crack front. The increase in toughness depends on the r_o/L ratio, where r_o is the radius of the precipitate and L is the inter-particle distance. However, this ratio is only a function of the precipitate volume fraction, and not of the precipitate size. Therefore, this mechanism does not contribute to the *R*-curve behavior.

Another toughening mechanism is when the crack is pinned by the precipitates and a higher stress is necessary for the crack to break away from them [28]. This model predicts a dependence of K_{IC} on the particle size and interparticle distance ratio between the precipitates. As the interparticle distance is proportional to the particle size, the increase in toughness due to this mechanism does not depend on the particle size. Therefore, the three mechanisms described above cannot explain the increase in fracture toughness with increasing crystal size.

Belli et al. [29] used the 3-point bending with eccentric notch (3-PBEN) test to investigate the fracture behavior of a pressable and a CAD/CAM LS2 glass-ceramic under combined mode-I and mode-II loading. The notches were made at a distance, *d*, from de midspan (S=16 mm): $d_0 = 0$ mm, $d_1 = 1.6$ mm, $d_2 = 3.2$ mm, $d_3 = 4.8$ mm, or $d_4 = 6.4$ mm, considering the phase angle, ψ, ranging from 0° for pure-mode I loading (d=0 mm) to 45° for K_I=K_{II}. The 3-PBEN test was useful for evaluating the mixed-mode fracture toughness of materials with up to 45° phase angle. Cracks encountering crystallites at 90° also deflected because of (i) higher fracture toughness of crystallites and (ii)

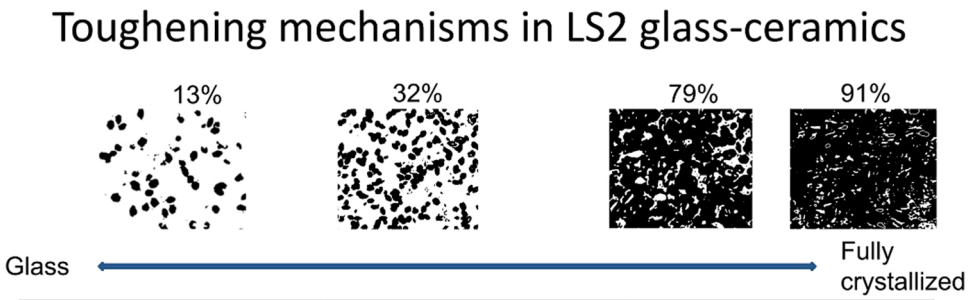

Glass matrix with isolated crystals	Two interpenetrating networks – glass and crystals	Crystalline matrix with isolated residual glass
• Higher residual stresses in the crystals • Crack deflection • Crack bowing • Crack trapping and bridging • Small contribution of $K_{IC}^{crystal}$ to overall toughness	• Approximately same residual stresses but different signs in the glass and crystals • Crack deflection • Crack bowing if the crystals are penetrable by cracks • Partial crack trapping and bridging • Crack bridging • Crystal fracture toughness contributes to overall K_{IC}	• Higher residual stresses in the glass • Crack deflection • Crack bridging • Strong contribution of $K_{IC}^{crystal}$ to overall toughness
• Crack follows the path according to the tensile components of the residual stress field in the glass and $K_{IC}^{crystal}/K_{IC}^{glass}$ ratio. • If crystals are cut, the crystal fracture toughness contributes to total toughness	• Crack follows mostly the tensile residual stress component in the glass-ceramic • Crack may penetrate the crystals depending on the $K_{IC}^{crystal}/K_{IC}^{glass}$ ratio	• Crack path tends to connect the glass islands
• Large crystals may promote spontaneous microcracking and R-curve behavior	• R-curve behavior	• Strong R-curve behavior • Larger crystals enhance R-curve, but large glass islands may promote microcracking

Fig. 13. Toughening mechanisms observed in LS2 GCs with increasing the crystallized volume fraction.

residual tensile stresses in the glass.

The increase of the fracture toughness with crystallized volume fraction observed in Fig. 7 is almost linear for the three crystal sizes. Assuming a simple rule of a mixture involving the work performed per unit area for fracturing the residual glass and the precipitates leads to:

$$K_{IC}^{gc} = K_{IC}^{glass}\sqrt{\frac{E_{gc}}{E_{glass}} + f\left(\frac{E_{gc}}{E_{crystal}}\left(\frac{K_{IC}^{crystal}}{K_{IC}^{glass}}\right)^2 - \frac{E_{gc}}{E_{glass}}\right)} \quad (9)$$

where K_{IC} and E are the fracture toughness and elastic modulus of each phase. The subscripts indicate glass (g), crystal and glass-ceramic (gc) [8]. This relation indicates a linear relation between K_{IC}^{gc} and f because E_{gc} depends also linearly with f. Therefore, the main toughening mechanism in these LS2 GCs is the crystallization of a tougher crystalline phase. The linear dependence arises from the increase of the surface area fractured of the crystalline phase and the increased elastic modulus of the glass-ceramic.

4.2.1. R-Curve behavior

Fig. 7 shows that K_{IC} increases with increasing crystal size. This is the main sign of *R*-curve behavior when elastic energy is dissipated as the crack propagates [30,31]. Crack bridges are observed in LS2 GCs, as shown in Fig. 12(c) and (f). The *R*-curve depends on crack size, crack and sample geometries, as well as on the type of test used. *R*-curve behavior has been studied extensively in ceramics, such as alumina [32,33] however, studies on the *R*-curve in GCs are scarce.

For instance, Vekinis et al. [33] studied the *R*-curve behavior of alumina. They derived expressions for three factors that affect the *R*-curve. The first is the stored elastic energy of the unbroken ligaments between the crack faces up to fracture. The increase in toughness due to this mechanism is:

$$\Delta K = \sigma_S\sqrt{\frac{f.d}{18(1-\nu^2)}}. \quad (10)$$

The second is the energy dissipated as a result of the friction of the crystal that bridges the crack faces. In this case, the increase in toughness is given by:

$$\Delta K = \sqrt{\frac{\mu E}{2(1-\nu^2)}\sigma_P.f.d}, \quad (11)$$

where μ is the friction coefficient of the grain and σ_P is the average stress that one crystal or the glass matrix exerts on the faces of the bridging crystal. It can be considered as the average thermal residual stress.

The third mechanism is the rotation of the crystal that bridges the crack faces during fracture, causing microcracking and friction. The increase in fracture toughness is:

$$\Delta K = \sqrt{\frac{\mu E}{4(1-\nu^2)}\sigma_S.f.d}. \quad (12)$$

In that study, the second and third mechanisms were the most important for the *R*-curve of alumina. As shown in Fig. 12, all three mechanisms are observed in LS2 GCs.

All mechanisms predict a dependence on the increase of K_{IC} due to *R*-curve proportional to $\sqrt{f.d}$. To test this dependence, we replotted the data of Fig. 7 as Fig. 14(a) by grouping the data with constant crystallized volume fraction and displaying the variation of K_{IC} with $d^{1/2}$. The lines are the best linear fit by the least squares method. As f increases, the angular coefficient of the lines determined by linear regression, m, increases. According to Eqs. (9)–(11), this increase should be proportional to $f^{1/2}$ for a constant d. Fig. 14(b) displays the variation of m with f in log scale. The line is the best linear fit and the calculated inclination is

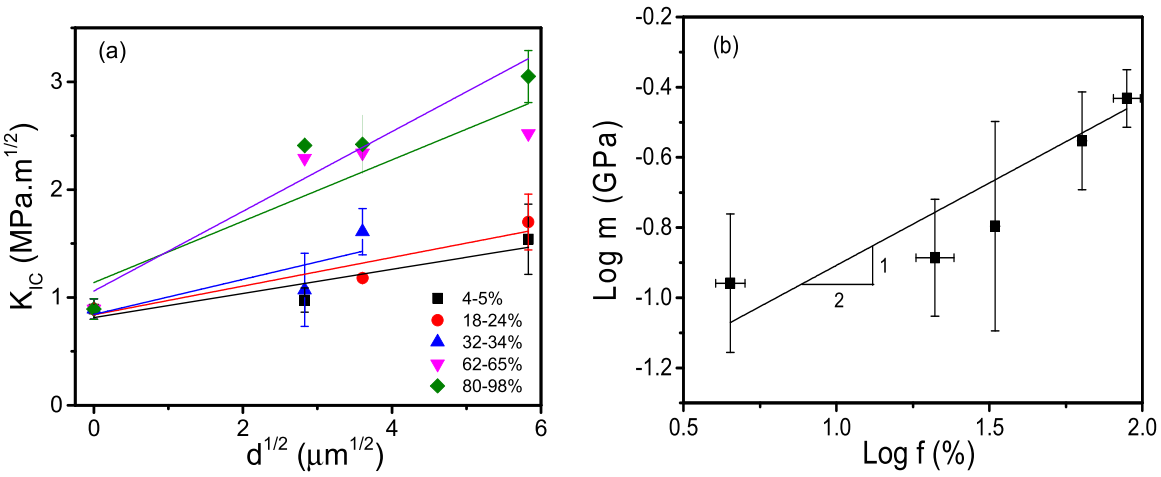

Fig. 14. Variation of (a) fracture toughness with crystal size for a constant crystallized volume fraction and (b) angular coefficient of lines in (a) with crystalized volume fraction.

0.5 ± 0.1. This is the value predicted by the Eqs. (9)–(11).

Materials exhibiting *R*-curve behavior are characterized by an increase in fracture toughness as the crack starts to grow, until a fully developed and stable bridging zone is established behind the crack and the fracture toughness reaches a constant value. In LS2 GCs, the length of the stable bridging zone is ~70 μm [34]. Evidence of lower fracture toughness for dental LS2-based GCs with submicron crystals was also reported. Recently, Lubauer et al. [35] investigated the *R*-curve behavior of three commercial LS2 dental materials. They used an indirect approach based on the relationship between strength and initial crack size obtained from quasi-static fracture toughness tests, using the 4-point bending technique with pre-cracks of different sizes produced by Knoop indentations. To obtain the values of the intensity factor of the onset of stable crack extension, $K_{I,0}$, they used a microcantilever specimen with a sharp notch produced by focused-ion-beam milling. They observed that crystalline fraction, crystals with higher aspect ratios, and crystal orientation perpendicular to the direction of crack propagation result in stronger *R*-curves.

The strong increase in K_{IC} for the GC with 34 μm at low *f*, which is not observed for the 8 and 13 μm crystals, is an indication of *R*-curve behavior present for larger precipitates and low volume fractions.

Finally, Sabino et al. [9] also obtained higher K_{IC} values for larger crystal sizes and crystallized volumetric fraction in $BaO.2SiO_2$ GCs, indicating that the *R*-curve might be present in many GC systems. The increase of K_{IC} al low f for the larger crystal. This finding warrants further investigation.

5. Summary and conclusions

To the best of our knowledge, this is the first study that characterized the mechanical properties of LS2 GCs varying the crystallized fraction and the grain size *independently*. Crystallization significantly increases both the fracture toughness and strength of these GCs. For a given volume fraction transformed, increasing crystal size increases the fracture toughness, but decreases the strength. Changing the average crystal size from 8 to 34 μm for a fully crystallized sample results in an increase of 45 % in the fracture toughness and a decrease of 23 % in strength. This is indicative of *R*-curve behavior.

The mechanical strength is controlled by critical flaws in the glass matrix, whose size is controlled by the crystal mean free path. A linear dependence of K_{IC} with *f* is observed, hence the main toughening mechanism in these LS2 GCs is the crystallization of a tougher crystalline phase. The contribution of *R*-curve mechanisms to the toughness increase is proportional to $(f.d)^{1/2}$, which agrees with *R*-curve models for ceramics.

These results shed light on some crucial features that are useful for the design of strong and tough GCs.

Declaration of Competing Interest

The authors declare that they have no known competing financial interests or personal relationships that could have appeared to influence the work reported in this paper.

Acknowledgments

The authors are grateful to the Brazilian funding agencies CNPq, CAPES, Fundação Araucária, São Paulo Research Foundation, CEPID-FAPESP grant no. 2013/07793-6 for the financial support, and to C-LABMU/UEPG and LaMaV/UFSCar for the use of their research facilities.

References

[1] E.D. Zanotto, A Bright future for glass-ceramics, Am. Ceram. Soc. Bull. 89 (2010) 19–27.
[2] M.J. Davis, E.D. Zanotto, Glass-ceramics and realization of the unobtainable: property combinations that push the envelope, MRS Bull. 42 (3) (2017) 195–199, https://doi.org/10.1557/mrs.2017.27.
[3] P.C. Soares, E.D. Zanotto, V.M. Fokin, H. Jain, TEM and XRD study of early crystallization of lithium disilicate glasses, J. Non Cryst. Solids 331 (1–3) (2003) 217–227, https://doi.org/10.1016/j.jnoncrysol.2003.08.075.
[4] P.F. James, Kinetics of crystal nucleation in silicate glasses, J. Non Cryst. Solids 73 (1–3) (1985) 517–540, https://doi.org/10.1016/0022-3093(85)90372-2.
[5] M.L.F. Nascimento, E.Dutra Zanotto, Does viscosity describe the kinetic barrier for crystal growth from the liquidus to the glass transition? J. Chem. Phys. 133 (17) (2010) 1–10, https://doi.org/10.1063/1.3490793.
[6] E.D. Mastelaro, V.R. Zanotto, Residual Stresses in a soda-lime-glass-ceramic, Joumal Non-Cryst. Solids 194 (1996) 297–304.
[7] H. Pinto, et al., Surface and bulk residual stresses in Li2O·2SiO2 glass-ceramics, J. Non Cryst. Solids 353 (24–25) (2007) 2307–2317, https://doi.org/10.1016/j.jnoncrysol.2007.04.007.
[8] F.C. Serbena, I. Mathias, C.E. Foerster, E.D. Zanotto, Crystallization toughening of a model glass-ceramic, Acta Mater. 86 (2015) 216–228, https://doi.org/10.1016/j.actamat.2014.12.007.
[9] S.R.F. Sabino, B.G.B. Cordeiro, L.D. Silva, A.G.M. Pukasiewicz, E.D. Zanotto, F. C. Serbena, Decoupling microstructural and residual stress effects on glass-ceramic toughening, Chem. Eng. eJournal (2022).
[10] R. Danzer, W. Harrer, P. Supancic, T. Lube, Z. Wang, A. Börger, The ball on three balls test-strength and failure analysis of different materials, J. Eur. Ceram. Soc. 27 (2–3) (2007) 1481–1485, https://doi.org/10.1016/j.jeurceramsoc.2006.05.034.
[11] E.D. Zanotto, P.F. James, Experimental tests of the classical nucleation theory for glasses, J. Non-Cryst. Solids 74 (1985) 373–394.
[12] R. Morrell, Fracture toughness testing for advanced technical ceramics: internationally agreed good practice, Adv. Appl. Ceram. 105 (2) (2006) 88–98, https://doi.org/10.1179/174367606×84422.

[13] V.M. Fokin, E.D. Zanotto, N.S. Yuritsyn, J.W.P. Schmelzer, Homogeneous crystal nucleation in silicate glasses: a 40 years perspective, J. Non Cryst. Solids 352 (26–27) (2006) 2681–2714, https://doi.org/10.1016/j.jnoncrysol.2006.02.074.
[14] P.C. Scares, C.M. Lepienski, Residual stress determination on lithium disilicate glass-ceramic by nanoindentation, J. Non Cryst. Solids 348 (2004) 139–143, https://doi.org/10.1016/j.jnoncrysol.2004.08.139.
[15] I. Mathias, Caracterização Mecânica e Transição Frágil-dúctil em Materiais Vitrocerâmicos, Univ. Estadual De. Ponta Gross (2015).
[16] D. Li, J.W. Guo, X.S. Wang, S.F. Zhang, L. He, Effects of crystal size on the mechanical properties of a lithium disilicate glass-ceramic, Mater. Sci. Eng. A 669 (2016) 332–339, https://doi.org/10.1016/j.msea.2016.05.068.
[17] S. Huang, P. Cao, C. Wang, Z. Huang, W. Gao, Fabrication of a high-strength lithium disilicate glass-ceramic in a complex glass system, J. Asian Ceram. Soc. 1 (1) (2013) 46–52, https://doi.org/10.1016/j.jascer.2013.02.007.
[18] M.O.C. Villas-Boas, F.C. Serbena, V.O. Soares, I. Mathias, E.D. Zanotto, Residual stress effect on the fracture toughness of lithium disilicate glass-ceramics, J. Am. Ceram. Soc. 103 (1) (2020) 465–479, https://doi.org/10.1111/jace.16664.
[19] G. Wen, X. Zheng, L. Song, Effects of P2O5 and sintering temperature on microstructure and mechanical properties of lithium disilicate glass-ceramics, Acta Mater. 55 (10) (2007) 3583–3591, https://doi.org/10.1016/j.actamat.2007.02.009.
[20] S. Massardo, Nanoindentação em vitrocerâmicas de dissilicato de lítio- Fractografia e propriedades mecânicas. UFPR (2011).
[21] F.C. Serbena, E.D. Zanotto, Internal residual stresses in glass-ceramics: a review, J. Non Cryst. Solids 358 (6–7) (2012) 975–984, https://doi.org/10.1016/j.jnoncrysol.2012.01.040.
[22] T. Mori, K. Tanaka, Average stress in matrix and average elastic energy of materials with misfitting inclusions, Acta Met. 21 (5) (1973) 571–574, https://doi.org/10.1016/0001-6160(73)90064-3.
[23] C.H. Hsueh, P.F. Becher, Residual thermal stresses in ceramic composites, part II: With short fibers, Mater. Sci. Eng. A 212 (1) (1996) 29–35, https://doi.org/10.1016/0921-5093(96)10177-5.
[24] J.C. Newman, I.S. Raju, An empirical stress-intensity factor equation for the surface crack, Eng. Fract. Mech. 15 (1–2) (1981) 185–192, https://doi.org/10.1016/0013-7944(81)90116-8.
[25] D.J. GREEN, Stress-induced microcracking at second-phase inclusions, J. Am. Ceram. Soc. 64 (3) (1981) 138–141, https://doi.org/10.1111/j.1151-2916.1981.tb10244.x.
[26] K.T. Faber, A.G. Evans, Crack deflection processes-I. Theory, Acta Met. 31 (4) (1983) 565–576, https://doi.org/10.1016/0001-6160(83)90046-9.
[27] A.F. Bower, M. Ortiz, A three-dimensional analysis of crack trapping and bridging by tough particles, J. Mech. Phys. Solids 39 (6) (1991) 815–858, https://doi.org/10.1016/0022-5096(91)90026-K.
[28] D.J. Green, Fracture toughness predictions for crack bowing in brittle particulate composites, J. Am. Ceram. Soc. 66 (1) (1983) C-4–C-5, https://doi.org/10.1111/j.1151-2916.1983.tb09975.x.
[29] R. Belli, M. Wendler, A. Petschelt, U. Lohbauer, Mixed-mode fracture toughness of texturized LS2 glass-ceramics using the three-point bending with eccentric notch test, Dent. Mater. 33 (12) (2017) 1473–1477, https://doi.org/10.1016/j.dental.2017.09.008.
[30] A.G. Evans, Perspective on the development of high-toughness ceramics, J. Am. Ceram. Soc. 73 (2) (1990) 187–206, https://doi.org/10.1111/j.1151-2916.1990.tb06493.x.
[31] R.F. COOK, B.R. LAWN, C.J. FAIRBANKS, Microstructure-strength properties in ceramics: I, effect of crack size on toughness, J. Am. Ceram. Soc. 68 (11) (1985) 604–615, https://doi.org/10.1111/j.1151-2916.1985.tb16163.x.
[32] R.W. Steinbrech, A. Reichl, W. Schaarwächter, R-curve behavior of long cracks in alumina, J. Am. Ceram. Soc. 73 (7) (1990) 2009–2015, https://doi.org/10.1111/j.1151-2916.1990.tb05260.x.
[33] G. Vekinis, M.F. Ashby, P.W.R. Beaumont, R-curve behaviour of Al2O3 ceramics, Acta Metall. Mater. 38 (6) (1990) 1151–1162, https://doi.org/10.1016/0956-7151(90)90188-M.
[34] U. Lubauer, J. Belli, R. Peterlik, H. Hurle, K. Lohbauer, Grasping the lithium hype: insights into modern dental lithium silicate glass-ceramics, Dent. Mater. 38 (2022) 318–332.
[35] U. Lubauer, J. AST, J. Goken, M. Merle, B. Lohbauer, Resistance-curve envelopes for dental lithium dissilicate glass-ceramic, J. Eur. Ceram. Soc. 42 (2022) 2516–2522.